New insight into the evolution of the vertebrate respiratory system and the discovery of unidirectional airflow in iguana lungs

Robert L. Cieri[a], Brent A. Craven[b], Emma R. Schachner[a], and C. G. Farmer[a,1]

[a]Department of Biology, University of Utah, Salt Lake City, UT 84112; and [b]Applied Research Laboratory, Department of Mechanical and Nuclear Engineering, The Pennsylvania State University, University Park, PA 16802

Edited by Neil H. Shubin, The University of Chicago, Chicago, IL, and approved October 17, 2014 (received for review March 19, 2014)

The generally accepted framework for the evolution of a key feature of the avian respiratory system, unidirectional airflow, is that it is an adaptation for efficiency of gas exchange and expanded aerobic capacities, and therefore it has historically been viewed as important to the ability of birds to fly and to maintain an endothermic metabolism. This pattern of flow has been presumed to arise from specific features of the respiratory system, such as an enclosed intrapulmonary bronchus and parabronchi. Here we show unidirectional airflow in the green iguana, a lizard with a strikingly different natural history from that of birds and lacking these anatomical features. This discovery indicates a paradigm shift is needed. The selective drivers of the trait, its date of origin, and the fundamental aerodynamic mechanisms by which unidirectional flow arises must be reassessed to be congruent with the natural history of this lineage. Unidirectional flow may serve functions other than expanded aerobic capacity; it may have been present in the ancestral diapsid; and it can occur in structurally simple lungs.

diapsid | evolution | lung | lizard | respiratory system

Energetically demanding forms of locomotion, such as powered flight, require a great capacity for gas exchange and selection for aerobic stamina may underlie many unique features of the avian respiratory system (1, 2). The avian respiratory system consists of highly vascularized lungs and avascular air sacs, which are membranous structures that effect ventilation and, in some species, extend between the muscles and even enter the bones (3). The topography of the conducting airways is complex; they form a circular system of tubes, analogous to the loop formed by the blood circulatory system in which arteries connect to veins through numerous small diameter vessels, the capillaries. Likewise, the avian conducting airways connect to each other through numerous tubules, the parabronchi, to form a circular path for respiratory gases (3). Gases flow through most of the parabronchi in the same direction during both inhalation and exhalation (unidirectional flow). This is due to the presence of aerodynamic valves (4–10). In contrast, the mammalian conducting airways arborize with the branch tips ending in blind sacs, there are no valves, and gases travel in the opposite direction along the conducting airways during expiration from the direction followed during inspiration (tidal flow). The presence of aerodynamic valves and unidirectional flow has generally been thought to be a highly derived feature found, among extant animals, only in birds and having evolved either in the crown group with flight or somewhere along the saurischian lineage leading to birds (11), perhaps as a mechanism to meet the high energetic demands of endothermy.

The discovery of unidirectional flow in the lungs of alligators (12, 13) and the savannah monitor lizard (14) indicates that we do not understand the distribution of this phenomenon among different lineages of vertebrates and raises questions about its underlying value. It is possible that unidirectional flow evolved convergently in crocodilians and monitor lizards and serves to expand aerobic capacity. Although monitor lizards are ectotherms, their lifestyles are largely convergent with small predatory mammals (15) and they have high aerobic capacities compared with other lizards (16). In contrast, extant alligators have limited aerobic stamina (17) but their common ancestor with birds may have had a great aerobic capacity (18) or may have been endothermic (19, 20). Crocodilians and monitor lizards also share a suite of features of their pulmonary and cardiac anatomy that have been purported to give rise to, or coevolve with, birdlike patterns of flow. These features are: (*i*) a bronchus that has grown deep into the lung as a mesobronchium, (*ii*) partitioning of the respiratory system into a mechanical part that functions in ventilation and a gas-exchanging region, (*iii*) intercameral perforations, and (*iv*) separation of the heart into right and left sides (1, 21). Crocodilians and monitors are also derived in having evolved mechanisms to supplement costal ventilation while exercising (18, 22, 23). Thus, unidirectional flow in these lineages may be one of many derived traits underpinning exceptionally high rates of oxygen consumption during activity.

It is also possible, however, that this pattern of flow evolved before the split of Diapsida into the Lepidosauromorpha (tuatara, lizards, snakes) and Archosauromorpha (crocodilians and birds) in an ectothermic ancestor lacking expanded aerobic capacities and living as long ago as the Permian Period. Unidirectional flow has been purported to serve ectotherms by harnessing the heart as a pump for air during periods of breath-holding (apnea) (12). Light can be shed on this pattern of evolution with observations of more squamates (snakes, lizards), which are the most diverse and largest (~9,000 species) group of living reptiles (24).

Significance

The avian respiratory system appears strikingly distinct from all other animals. Purported key innovations underpinning avian patterns of airflow are an enclosed intrapulmonary bronchus, intercameral perforations, heterogeneous parenchyma; these traits allegedly coevolved with separation of the cardiac ventricle into right and left sides and are presumed to have been favored by selection because they facilitate high activity metabolisms. In contradistinction to these prevailing theories, here we show that unidirectional flow is present in the lungs of the green iguana, an ectothermic animal with low aerobic capacity, no intrapulmonary bronchus, and no intercameral perforations. This discovery indicates a transformation in our understanding of the evolution of the vertebrate respiratory system is needed.

Author contributions: C.F. designed research; R.L.C., B.A.C., E.R.S., and C.F. performed research; R.L.C., B.A.C., and C.F. analyzed data; B.A.C. and C.F. contributed new reagents/analytic tools; and B.A.C. and C.F. wrote the paper.

The authors declare no conflict of interest.

This article is a PNAS Direct Submission.

[1]To whom correspondence should be addressed. Email: cg.frmr@gmail.com.

This article contains supporting information online at www.pnas.org/lookup/suppl/doi:10.1073/pnas.1405088111/-/DCSupplemental.

To test the hypothesis that unidirectional flow is present in squamates other than varanid lizards; to better understand anatomical features that give rise to these patterns of flow; and to gain insight into the underlying value of this pattern of flow, green iguanas (*Iguana iguana*) were studied. Green iguanas differ from monitors because they are herbivores and because they have structurally simple lungs that lack an enclosed intrapulmonary bronchus. Iguanas lack septation of the cardiac ventricle and have poor locomotor stamina. The poor stamina is due in part from an impairment during running in their blood and air circulatory systems (19, 25, 26).

Results

Iguana lungs are simple, large, paired organs that occupy much of the thoracoabdominal cavity; each lung is partitioned by a septum into a small cranial chamber and a much larger caudal chamber (Fig. 1*A*). The primary bronchus enters into the cranial chamber of the lung from a ventromedial aspect along an oblique trajectory, coursing laterally, caudally, and dorsally. The hilus is located approximately one-third the length of the cranial chamber from its apex and near the most cranial section of the caudal chamber (Fig. 1). The dorsal half of the primary bronchus terminates at the hilus, whereas the ventral half, still containing partial rings of cartilage, flattens and continues distally to form part of the septum separating the chambers (Fig. 1*B*). A single oval ostium in the floor of the flattened bronchus connects the chambers (Fig. 1*C*). Otherwise, the septation between the cranial and caudal chamber is airtight (no intercameral perforations are present; $n = 5$). Partial septa line portions of the walls of the lungs forming pockets. These pockets are especially numerous where the heart and lungs are contiguous and along the septum separating the two chambers (Fig. 1*A*).

In both chambers unidirectional flow occurred in vivo ($n = 5$). Throughout the respiratory cycle, insufflated, aerosolized lipids flowed craniad along portions of the walls of the lungs in both chambers whereas caudally directed flow was primarily confined to the inspiratory phase and was mostly located in high-speed streams emanating in the cranial chamber from the bronchus and in the caudal chamber from the ostium (Fig. 2 and Movies S1 and S2). Unidirectional flow could not have been generated by the activity of sphincters or other muscular valves because it was also observed in excised lungs under the following two conditions. First, flow was visualized in excised lungs that had been filled with water containing pollen, microspheres, or citrus pulp ($n = 5$). The water was injected and withdrawn through the trachea and the movement of particles within the lungs imaged under a dissecting scope (Fig. 3 and Movie S3). Second, recordings from heated thermistor flow meters ($n = 10$) that were implanted in the walls of the lungs in situ and in excised lungs (separate experiments) confirmed the pattern of airflow observed in vivo (Fig. 4).

Simulated patterns of flow corroborated the data collected in vivo and in excised lungs and provided insight into the detailed patterns of flow (Figs. 2–5 and Movies S4 and S5). During inspiration, both the simulations and our visualization of smoke in air and particles in water showed that fluid formed high-speed streams (or jets) as it entered both the cranial and caudal chambers as the lungs expanded. These streams entered the chambers medially and flowed laterocaudad. During exhalation, fluid was pushed out of each chamber with relatively slow speed and, in the caudal chamber, moved primarily craniad along the long axis of the body. Therefore, in the region of the inspired, high-speed fluid stream, the flow was tidal. However, in regions that lie outside the fluid stream, fluid flowed primarily craniad during inspiration and expiration (Figs. 2–4 and Movies S1–S3 and S5).

Discussion

The pattern of flow in the simple lungs of the green iguana is strikingly similar in many ways to the pattern of flow seen in the more complex lungs of birds, crocodilians, and varanid lizards. By a simple streaming of the fluid, tidal flow occurs in the iguana

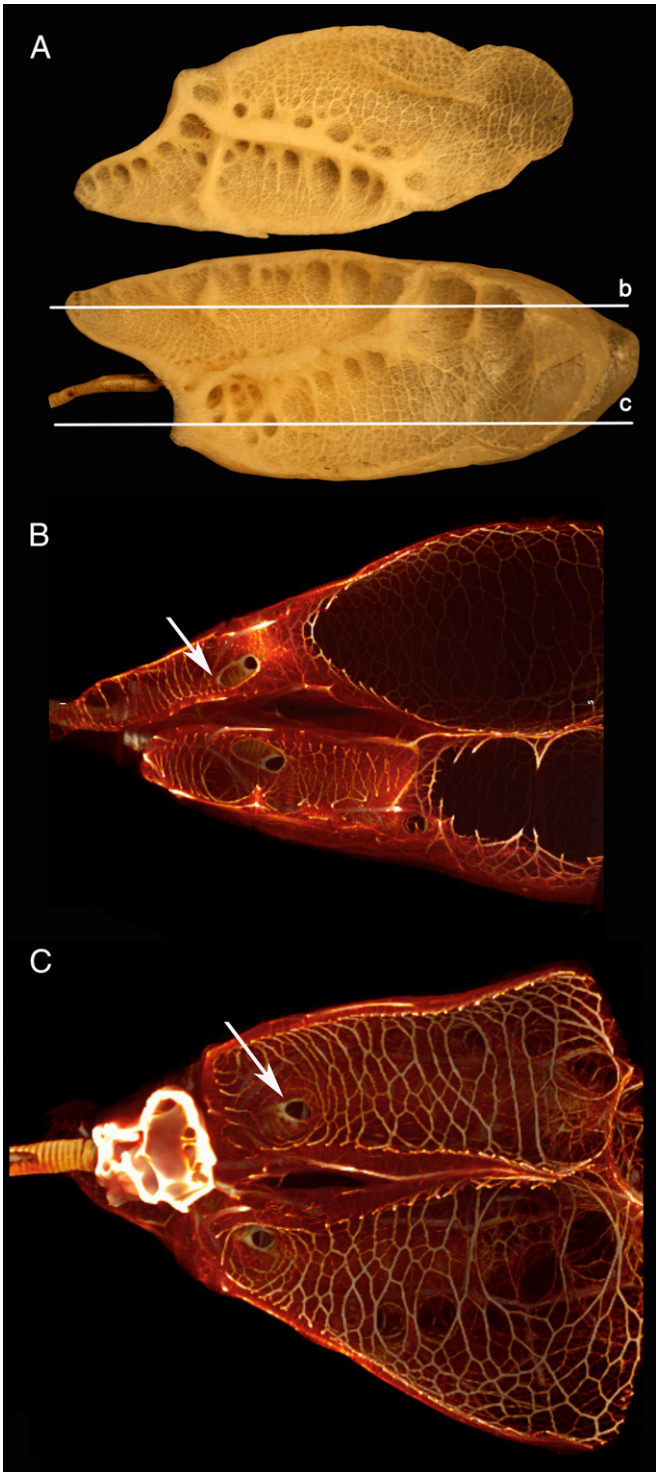

Fig. 1. Anatomy of the respiratory system of the green iguana. (*A*) Dried left lung transected in the parasagittal plane (cutaway section inverted). White lines (b and c) mark approximate levels of transection shown in volume-rendered μCT data illustrated in *B* and *C*. (*B*) Dorsal view of both lungs transected in the coronal plane. Arrow points to the location where the primary bronchus enters the cranial chamber of the right lung. (*C*) Ventral view of the three chambered heart and lungs transected in the coronal plane. Arrow marks the ostium between the chambers of the left lung. Craniad, left.

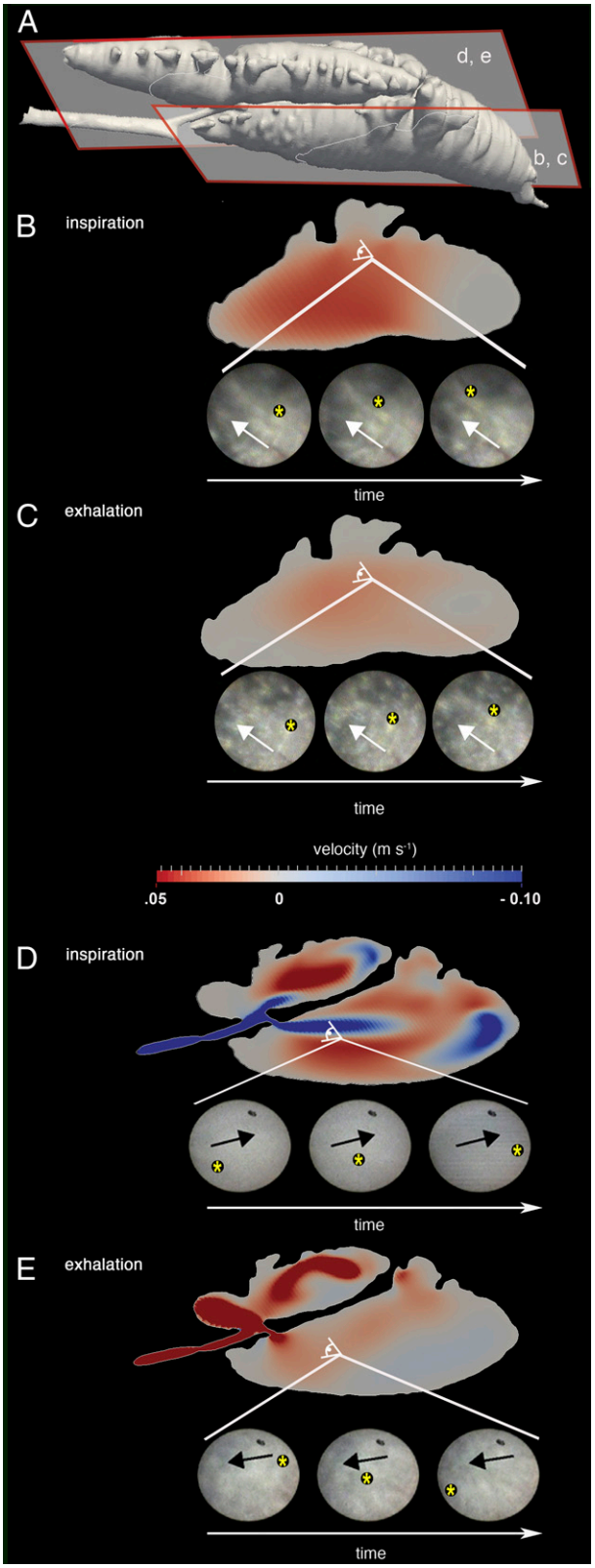

Fig. 2. Flow simulation and in vivo visualization of smoke. (*A*) Dorsomedial view of the model with planes of section (b,c and d,e) projected in *B*–*E*. (*B*) Inspiration: Simulated flow in plane b,c is primarily craniad (warm colors). Eye marks approximate location where smoke (circles) was visualized in vivo (Movie S1). Smoke flows craniad at this location. (*C*) Exhalation: simulated flow and visualized smoke move craniad. (*D*) Inspiration: simulated flow in plane d,e shows high-speed fluid streams emanating caudad (cool colors) from the primary bronchus and ostium. Smoke flows caudad (Movie S2). (*E*) Exhalation: Simulated and visualized flow is craniad. Flow velocity (meters per second). Note the change in direction as denoted by the arrows. Asterisk, a clump of smoke.

lung in the central portion of the chambers despite the absence of enclosed intrapulmonary bronchi, whereas primarily unidirectional flow occurs elsewhere along many of the walls, where the gas-exchange blood vessels are located, despite the absence of intercameral perforations or parabronchi.

These results indicate that unidirectional flow does not require either a bronchus that has grown deep into the lung as a mesobronchium or intercameral perforations. Furthermore, these results show that unidirectional flow does not necessarily coevolve with separation of the heart into the left and right sides, as has been proposed (1). Although an enclosed intrapulmonary bronchus, intercameral perforations or parabronchi, and a large degree or total separation of the heart are found in archosaurs and monitor lizards (1, 27), none of these features are present in the green iguana (Fig. 1).

This discovery corroborates the evolutionary scenario that unidirectional flow was present in Diapsida before the split of this lineage into the Archosauromorpha and the Lepidosauromorpha, dating its origin to at least the Permian Period. However, convergent evolution has not been ruled out, and more research is needed assessing patterns of flow in the tuatara, snakes, and other lizards, turtles, amphibians, and lung-breathing fishes. The results of this study also suggest that unidirectional flow is not an adaptation for expanding aerobic capacity and did not arise coincident with vigorous sustained locomotion or with endothermy. Other selective pressures for the forerunner of the avian lung should be investigated (12). The presence of unidirectional flow in the ancestral diapsid would be permissive to the evolution of efficacious countercurrent and crosscurrent gas exchangers, such as those found in the gills of fish and the lungs of birds. However, we know of no clear evidence for increased efficiency of gas exchange in nonavian reptiles over that seen in mammals, for example, ventilation-perfusion matching during exercise in the savannah monitor is very similar to that of many mammals (28). Nevertheless, more studies of the patterns of blood flow relative to airflow and of blood gases relative to lung gases in iguanas and other diapsids will be important in shedding light on the functional underpinning for the evolution of this pattern of flow and on the evolutionary history of the vertebrate respiratory system.

Materials and Methods

In Vivo Experiments. Experiments were performed in accordance with the University of Utah Animal Care and Use Committee. Animals weighed between 0.2 and 1.6 kg. Intrapulmonary airflow was visualized in vivo (n = 5) using an endoscope with a diameter of 0.9 mm (Model number HSF 009 1000 NVK, Hawkeye Pro Microflex Boroscope, Gradient Lens Corporation) and with a field of view of 55 degrees. The endoscope was implanted under anesthetic in three locations in order for the majority of the lung to be monitored. The locations were chosen to provide as many views of the lung as possible. The endoscope entered through an incision in a distal portion of the caudal chamber (n = 3), (Fig. 6 *A* and *B*) and was advanced craniad and caudad, providing views of all aspects of the caudal chamber. Once these data were collected, the scope was advanced through the ostium between the caudal and cranial chambers. The field of view was restricted in the cranial chamber to the laterocranial aspect of the cranial chambers. In two animals, the probe was inserted into a cranial location of the respiratory system (through the glottis in one animal and through an incision in the trachea in the other) and advanced caudad into the cranial chamber, providing a larger field of view of the caudal aspect of the cranial chamber. Once the data were collected at this location, the probe was advanced through the ostium into the caudal chamber to provide a view of the caudal aspect of the caudal chamber. While the scope was held in one location, a synthetic smoke (Froggy's Fog – Swamp Juice, Froggys Fog) was delivered into the inspired air by a fog machine (Eliminator Lighting Fog Machine EL-400). The films of smoke moving within the lungs were captured using

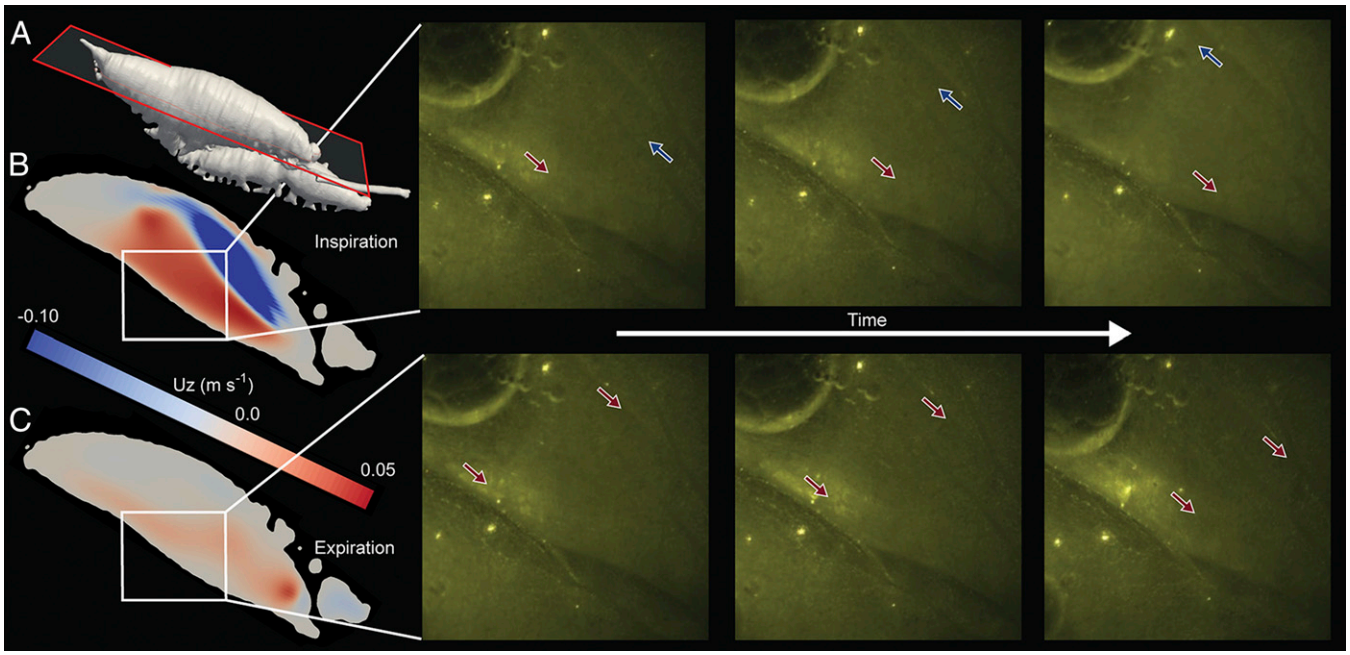

Fig. 3. Flow simulation and ex vivo visualization of flow. (*A*) Ventromedial view of model with coronal plane of section projected in *B* and *C*. (*B*) Inspiration: Simulation shows a high-velocity fluid stream emanating caudad (cool colors) and laterad with flow along the medial wall craniad (warm colors). White square marks the approximate location on the model where flow was visualized in excised lungs using fluorescent microspheres in water. Green square panels show three consecutive frames of video (Video S3) of microspheres moving in the lungs while fluid was injected (top three panels) and while it was withdrawn (bottom three panels). (*C*) Expiration: simulated flow is largely craniad. Flow magnitude (meters per second). Red and blue arrows track microspheres moving craniad and caudad respectively.

a Luxxor Video Camera System (LXX-VBSM), which was interfaced to a computer with a USB 2.0 Image Capture Interface (VC-USB2), and recorded with Debut Video Capture software. The rate of frame capture was 29.97 frames per second. For the purpose of making still images from the movies to display in the printed manuscript, clumps of smoke were tracked visually by advancing through the frames one at a time. The videos of moving smoke did not quantify distances that the particles moved. The videos provide evidence of direction of flow and a qualitative assessment of speed. The velocity of the smoke was not measured. Direction of airflow was determined visually. Both chambers were monitored in all five animals although the exact views differed depending on the location where the probe entered. A minimum of 20 breathing cycles was observed in each location studied. Airflow at the nares was measured with a pneumotachograph (Hans Rudolph) or dual heated thermistor flow meter (HEC 132C, Hector Engineering).

In Situ and ex Vivo Experiments. Airflow was measured in separate experiments in situ and in excised lungs ($n = 10$) by implanting a dual thermistor flow meter (HEC 132C, Hector Engineering) into both the dorsal and ventral chambers (Fig. 6). The trachea was intubated and the lung ventilated using a 60-cm^3 syringe. Tracheal flow was measured using a pneumotachograph (Hans Rudolph). The signal was amplified by an A.C./D.C. strain gauge amplifier (P122, Grass Instruments). All analog signals were converted to digital (Biopac Systems) with a sampling rate of 60 Hz and recorded on a computer using AcqKnowledge software (Biopac Systems).

Flow was visualized in excised lungs ($n = 5$) by intubating the trachea and filling the lungs with saline containing microspheres (222 μm in diameter, Thermo Scientific; or C14837, Invitrogen) or pollen collected from sunflowers (*Helianthus annuus*) or citrus pulp. Fluid was withdrawn or pushed into the lung using a 60-cm^3 syringe, and the movement of these particles was visualized using dissection scopes and filmed with a Canon EOS T2i (resolution of 1,080 pixels) digital camera.

Anatomical Methods. To assess the presence of intercameral perforations, the lungs ($n = 5$) were excised and the ventral chamber opened. The ostium between the cranial and caudal chambers was sealed with latex. After the latex cured, air was injected into the cranial chamber through the trachea or primary bronchus and the lung placed under water. Gentle pressure was applied manually to the cranial chamber and the intercameral septum was inspected visually for air bubbles filtering through the septum.

Microcomputed tomography (μCT) images of excised lungs that had been stained with a KI solution were acquired with an Inveon μCTscanner (Siemens Preclinical Solutions). Images consisted of 360 degrees rotation with 1,100 steps. The exposure time was 1,700 ms, with detector settings at 80 peak kilovolts and 200 μAmps and a filter of 0.5 mm. Data were reconstructed onto a 2,048 × 2,048 × 1,792 image matrix using the COBRA software package (Exxim Computing). The effective image pixel size was 28.56 μm. Reconstructed images were cropped and visualized using the Siemens Inveon Research Workplace (IRW) and OsiriX software.

Computed tomography data were collected on a Siemens Somatom Definition Flash Scanner at 100 peak kilovolts and 400 milliamp tube current. A series of images were acquired along the long axis of the body. The thickness of each image (slice) was 0.6 mm, and the slices were acquired at intervals of 0.4 mm along the long axis such that 0.2 mm of each slice overlapped with the previous slice. A surface model was then reconstructed from a manual segmentation of the CT data using Avizo 7.1 (www.vsg3d.com/avizo/standard) and a Wacom Intuos4 pen tablet.

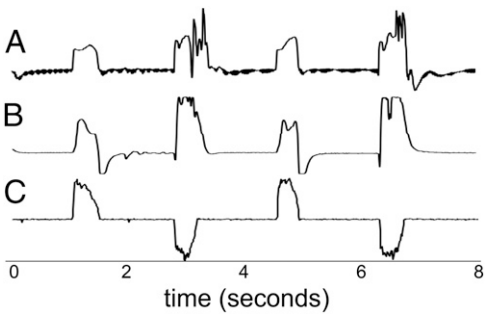

Fig. 4. Pulmonary and tracheal airflow in an excised lung. Direction of airflow measured along the walls of the lung with heated thermistor flow meters in the cranial chamber (*A*) and caudal chamber (*B*). Positive trace is cranial flow. (*C*) Direction of airflow in the trachea measured with a pneumotachograph. Positive trace is exhalation. Note air moved craniad in both chambers during both phases of ventilation.

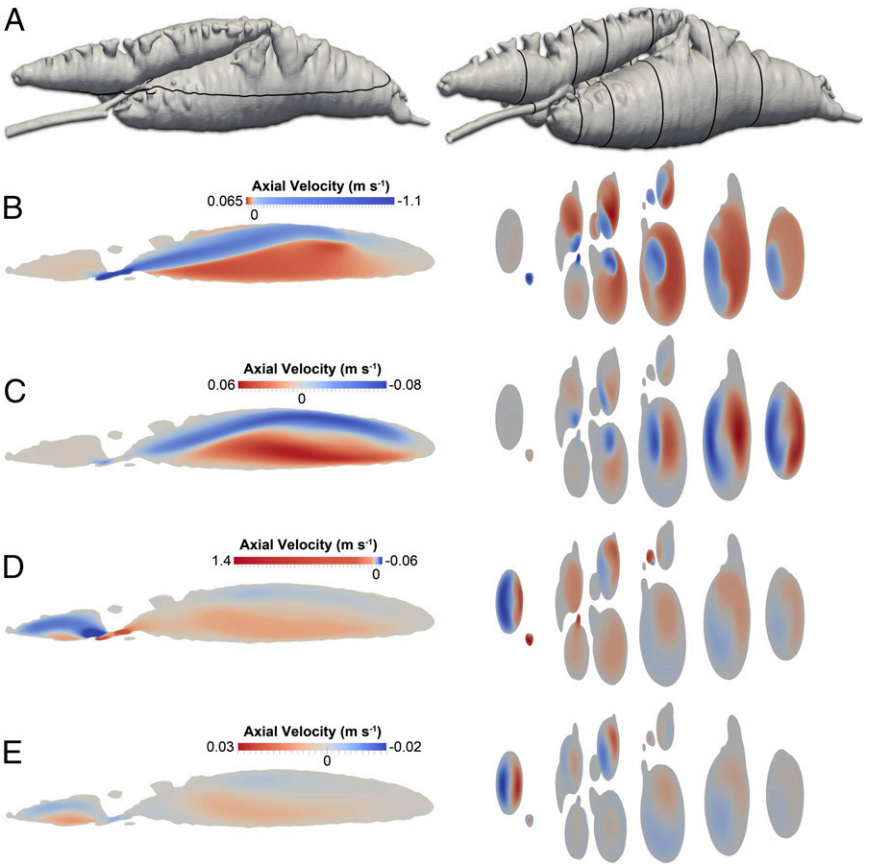

Fig. 5. Computational fluid dynamics simulation of airflow at four consecutive seconds in the respiratory cycle in coronal (*Left*) and transverse (*Right*) planes. (*A*) Medial views of the computational model with lines illustrating planes of view projected in *B*–*E*. (*B*) During peak flow of inspiration high-speed fluid streams emanate into both chambers laterocaudad. Most of the remainder of the flow is moving craniad. (*C*) One second later as inspiration ends and no bulk flow enters or exits the lungs, the internal flow recirculates in a laterocaudal to mediocranial direction. (*D*) During peak flow of exhalation most of the air flows craniad. (*E*) End of exhalation and no bulk flow enters or exits the lungs, but both chambers contain low-speed recirculating flow. Axial direction corresponds to the body axis.

Computational Fluid Dynamics Simulations. Airflow was simulated using the 3D surface model that was reconstructed from CT data of the right lung of a green iguana. Given the reconstructed surface model, a high-fidelity computational mesh consisting of approximately 1.8 million elements was generated using the hexahedral-dominant, unstructured mesh generation utility, snappyHexMesh, available in the open-source computational continuum mechanics library, OpenFOAM (www.openfoam.com). A computational fluid dynamics (CFD) simulation of respiratory airflow was carried out using the segregated pressure-based PIMPLE (hybrid PISO/SIMPLE) algorithm available in OpenFOAM to solve the time-accurate incompressible continuity and Navier–Stokes equations in an arbitrary Lagrangian–Eulerian (ALE) reference frame with dynamic mesh motion and second-order accurate temporal and spatial

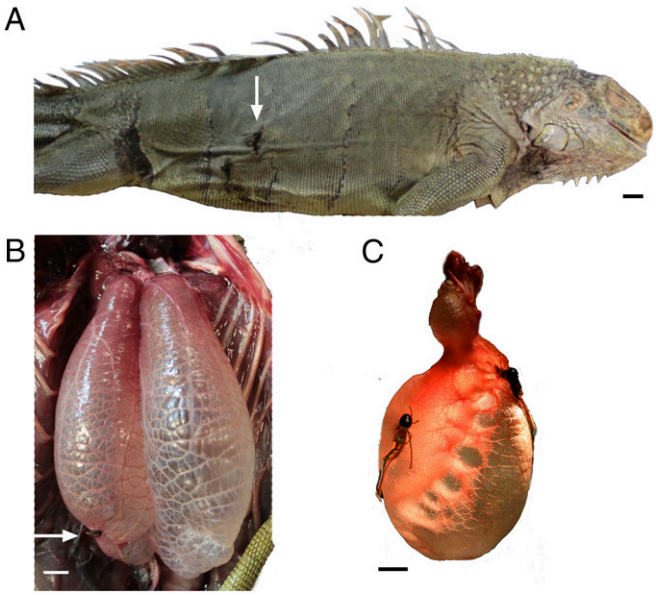

Fig. 6. Probe placement. (*A*) Right lateral view showing the caudal point of entry of the endoscope (white arrow). (*B*) Ventral view of lungs showing caudal point of entry of the endoscope (white arrow). (*C*) Lateral view of excised right lung showing location of thermistor flow meters. (Scale bar, 1 cm.)

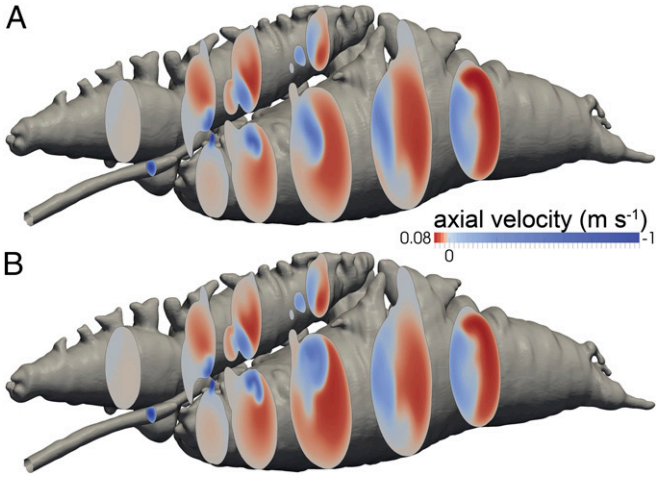

Fig. 7. Numerical verification of CFD solutions of airflow in the iguana lung. (*A*) Flow patterns in the iguana lung during inspiration computed using the coarser mesh (1.8 million elements) and time step (0.005 s). (*B*) Flow patterns at the same time as in *A* computed using the finer mesh (3.9 million elements) and time step (0.0005 s).

discretization schemes. No-slip boundary conditions were applied on the walls of the lung and a custom mesh motion boundary condition was developed to expand and contract the lung at a rate of 15 breaths per minute with a tidal volume of 11 mL, which was based on resting data for green iguanas (25). A physiologically realistic motion of the lung walls was prescribed to match in vivo observations of resting breathing. In particular, the caudal chamber was made to expand and contract more than the cranial chamber and the motion of both chambers was prescribed to be greater laterally than medially. A transient simulation of five breathing cycles was carried out to obtain a time-periodic steady state solution. The computation was performed on 96 processors of a high-performance parallel computer cluster at Penn State University. Airflow patterns in the lung were extracted directly from the numerical solutions using the open-source visualization software ParaView (www.paraview.org).

To ensure that the computational solution is independent of the mesh resolution and time step size, a second simulation was carried out using a significantly finer mesh and a much smaller time step. In particular, the finer mesh contained 3.9 million computational elements, more than twice the number of elements in the coarser mesh, and the simulation was performed on 192 processors using a time step size of 0.0005 s, an order of magnitude smaller than that used in the coarser simulation (0.005 s). In summary, the overall flow patterns in the lung for the coarse and fine mesh simulations are extremely similar (Fig. 7), thereby confirming that the reported results are mesh- and time step-independent.

ACKNOWLEDGMENTS. We thank James Butler for insightful conversations and inspiration. This work was funded by the National Science Foundation (IOS 0818973 and IOS 1055080, to C.G.F.).

1. Wolf S (1933) Zur kenntnis von Bau und Funktion der Reptilienlunge. *Zool. Jahrb. Abt. Anat. Ontol.* 57:139–190.
2. Maina JN (2000) What it takes to fly: The structural and functional respiratory refinements in birds and bats. *J Exp Biol* 203(Pt 20):3045–3064.
3. Duncker HR (1971) The lung air sac system of birds. A contribution to the functional anatomy of the respiratory apparatus. *Ergebn Anat EntwGesch* 45:1–171.
4. Hazelhoff EH (1951) Structure and function of the lung of birds. *Poult Sci* 30:3–10.
5. Butler JP, Banzett RB, Fredberg JJ (1988) Inspiratory valving in avian bronchi: Aerodynamic considerations. *Respir Physiol* 72(2):241–255.
6. Wang N, Banzett RB, Butler JP, Fredberg JJ (1988) Bird lung models show that convective inertia effects inspiratory aerodynamic valving. *Respir Physiol* 73(1):111–124.
7. Wang N, Banzett RB, Nations CS, Jenkins FA, Jr (1992) An aerodynamic valve in the avian primary bronchus. *J Exp Zool* 262(4):441–445.
8. Banzett RB, et al. (1987) Inspiratory aerodynamic valving in goose lungs depends on gas density and velocity. *Respir Physiol* 70(3):287–300.
9. Brackenbury JH (1971) Airflow dynamics in the avian lung as determined by direct and indirect methods. *Respir Physiol* 13(3):319–329.
10. Dotterweich H (1930) Versuch über den Weg der Atemluft in der Vogellunge. *Z Vgl Physiol* 11:271–284.
11. Perry SF (1992) Gas exchange strategies of reptiles and the origin of the avian lung. *Physiological adaptations in vertebrates; respiration, circulation, and metabolism*, eds Wood S, Weber R, Hargens A, Millard R (Marcel Dekker, Inc., New York), Vol 56, pp 149–167.
12. Farmer CG (2010) The provenance of alveolar and parabronchial lungs: Insights from paleoecology and the discovery of cardiogenic, unidirectional airflow in the American alligator (*Alligator mississippiensis*). *Physiol Biochem Zool* 83(4):561–575.
13. Farmer CG, Sanders K (2010) Unidirectional airflow in the lungs of alligators. *Science* 327(5963):338–340.
14. Schachner ER, Cieri RL, Butler JP, Farmer CG (2014) Unidirectional pulmonary airflow patterns in the savannah monitor lizard. *Nature* 506(7488):367–370.
15. Sweet SS, Pianka ER (2007) Monitors, mammals, and Wallace's Line. Third Multidisciplinary World Conference on Monitor Lizards, Alexander Koenig Museum, Bonn, Germany. *Mertensiella* 16:79–99.
16. Thompson GG, Withers PC (1997) Standard and maximal metabolic rates of goannas (Squamata:Varanidae). *Physiol Zool* 70(3):307–323.
17. Farmer CG, Carrier DR (2000) Ventilation and gas exchange during treadmill locomotion in the American alligator (*Alligator mississippiensis*). *J Exp Biol* 203(Pt 11):1671–1678.
18. Farmer CG, Carrier DR (2000) Pelvic aspiration in the American alligator (*Alligator mississippiensis*). *J Exp Biol* 203(Pt 11):1679–1687.
19. Carrier DR (1987) The evolution of locomotor stamina in tetrapods: Circumventing a mechanical constraint. *Paleobiology* 13:326–341.
20. Seymour RS, Bennett-Stamper CL, Johnston SD, Carrier DR, Grigg GC (2004) Evidence for endothermic ancestors of crocodiles at the stem of archosaur evolution. *Physiol Biochem Zool* 77(6):1051–1067.
21. Huxley TH (1882) On the respiratory organs of *Apteryx*. *Proc Zool Soc Lond* 1882: 560–569.
22. Owerkowicz T, Farmer CG, Hicks JW, Brainerd EL (1999) Contribution of the gular pump to ventilation. *Science* 284:1661–1663.
23. Gans C, Clark B (1976) Studies on ventilation of *Caiman crocodilus* (Crocodilia: Reptilia). *Respir Physiol* 26(3):285–301.
24. Wiens JJ, et al. (2012) Resolving the phylogeny of lizards and snakes (Squamata) with extensive sampling of genes and species. *Biol Lett* 8(6):1043–1046.
25. Wang T, Carrier DR, Hicks JW (1997) Ventilation and gas exchange in lizards during treadmill exercise. *J Exp Biol* 200(Pt 20):2629–2639.
26. Farmer CG, Hicks JW (2000) Circulatory impairment induced by exercise in the lizard *Iguana iguana*. *J Exp Biol* 203(Pt 17):2691–2697.
27. Hicks JW (1998) Cardiac shunting in reptiles: Mechanisms, regulation and physiological function. *Biology of the Reptilia*, eds Gans C, Gaunt AS (Society for the Study of Amphibians and Reptiles, Ithaca, NY), Vol G, pp 425–483.
28. Hopkins SR, Hicks JW, Cooper TK, Powell FL (1995) Ventilation and pulmonary gas exchange during exercise in the savannah monitor lizard (*Varanus exanthematicus*). *J Exp Biol* 198(Pt 8):1783–1789.